POLITECNICO DI TORINO
Repository ISTITUZIONALE

Stability analysis of a pneumatically actuated inverted pendulum

Original
Stability analysis of a pneumatically actuated inverted pendulum / Colombo, F.; Mazza, L.; Pepe, G.; Raparelli, T.; Trivella, A.. - In: E3S WEB OF CONFERENCES. - ISSN 2267-1242. - ELETTRONICO. - 197:(2020), p. 07008. (Intervento presentato al convegno 75th National ATI Congress - #7 Clean Energy for all, ATI 2020 tenutosi a ita nel 2020) [10.1051/e3sconf/202019707008].

Availability:
This version is available at: 11583/2883272 since: 2021-04-03T14:44:13Z

Publisher:
EDP Sciences

Published
DOI:10.1051/e3sconf/202019707008

Terms of use:

This article is made available under terms and conditions as specified in the corresponding bibliographic description in the repository

Publisher copyright

(Article begins on next page)

06 October 2024

Stability analysis of a pneumatically actuated inverted pendulum

*Federic*o Colombo, *Luigi* Mazza, *Giuseppe* Pepe, *Terenziano* Raparelli, *Andrea* Trivella

Politecnico di Torino, Technical University,
C.so Duca degli Abruzzi 24, 10129, Torino, Italy

Abstract. This paper deals with the stabilization of an inverted pendulum on cart; the latter is pneumatically actuated by a double acting cylinder controlled by low cost proportional valves. In particular, a numerical model of whole system is developed in order to find the ability of the pneumatic actuation in stabilizing the pendulum and evaluate its bandwidth. A cascade of two control loops (the inner one for the pendulum angle, the outer one for the cart displacement) are analyzed and proper compensators are defined. The possibility of introducing an additional loop to control the force exerted by the actuator on the cart is evaluated.

1 Introduction

Majority of the inverted pendulum based applications belong to the field of human transportation such as self-balancing scooters [1], unicycles [2] or electric motorbikes [3]; recently many solutions have grown in the version of "autonomous robots" [4-6]. The inverted pendulum still remains an interesting system for didactic use or to test new control types; to this aim papers focused on different architectures and control strategies [7, 8] can be found. Moreover, applications in the field of biomechanics are quite interesting and challenging; in particular, the gait modelling and stability of biped robots [9] and postural exoskeleton balancing [10] are based on inverted pendulum models. Most of the applications make use of electric actuators, appreciated for their high bandwidth. Anyway, some others make use of pneumatic technology [11-14], which presents some advantages such as the low cost and bandwidth sufficient to obtain stabilization. In [11] a low cost pneumatic actuator is used to control the system, together with potentiometers that measure the linear and angular displacements of cart and pendulum respectively. The control is implemented on a notebook equipped with a PCMCIA card. In [12] an inner loop controlling the actuating force of a pneumatic cylinder was studied, while position and angle were controlled in an outer loop. A friction estimator offsets the control signal for the force control to compensate for friction. However the work is purely numerical.

The authors have already designed and manufactured a prototype of inverted pendulum mounted on cart and pneumatically actuated. The architecture of the system is described [13, 14]. Four proportional valves were used to supply the double-acting cylinder and

© The Authors, published by EDP Sciences. This is an open access article distributed under the terms of the Creative Commons Attribution License 4.0 (http://creativecommons.org/licenses/by/4.0/).

potentiometers are employed to feedback the displacement signals; in particular, in [14] a common industrial logic controller (PLC) was used to control the pneumatic servosystem.

In this paper, the numerical model of the pneumatic system is detailed and various compensators are designed in order to achieve good stability margins and bandwidth. A cascade of two control loops (the inner one for the pendulum angle, the outer one for the cart displacement) is analysed and stability is discussed. The possibility of introducing an additional inner loop (third loop) to control the force exerted by the pneumatic cylinder is also evaluated and discussed.

2 Mathematical model

The inverted pendulum on cart is described by equations (1), (2) which represent the rotational and translational equilibrium:

$$g \sin \vartheta - l\ddot{\vartheta} + \ddot{x} \cos \vartheta = 0 \tag{1}$$

$$\left(m_p + m_c\right)\ddot{x} + m_p l\dot{\vartheta}^2 \, sin \, \vartheta - m_p l\ddot{\vartheta} \, cos \, \vartheta + b_c\dot{x} - F = 0 \tag{2}$$

After linearization of these equations, it is possible to obtain the transfer function between angle θ and cart position x

$$\frac{x(s)}{\theta(s)} = G_{x/\theta} = \frac{ls^2 - g}{s^2} \tag{3}$$

and the transfer function between the force F applied by the cylinder to the cart and angle θ:

$$\frac{\vartheta(s)}{F(s)} = G_{\theta/F} = \frac{s}{m_c ls^3 + b_c ls^2 - g\left(m_p + m_c\right)s - b_c g} \tag{4}$$

The pneumatic cylinder is modelled considering the equilibrium equation (5) and the mass balance equations (6, 7) for the two chambers (rear chamber A and front chamber B). Friction force in pneumatic actuators depends on many factors such as velocity, chambers pressure, greasing conditions, material and shape of the seals [15], which can lead to complex friction models. For the scope of this analysis, a classical viscous friction model was employed.

$$F = p_A A_A - p_B A_B - \, p_a(A_A - A_B) - b_p\dot{x} - M_p\ddot{x} \tag{5}$$

$$\dot{m}_A = \frac{\dot{p}_A \rho_0}{p_0}(V_{A0} + A_A x) + \frac{p_A \rho_0}{p_0} A_A \dot{x} \tag{6}$$

$$\dot{m}_B = \frac{\dot{p}_B \rho_0}{p_0}(V_{B0} - A_B x) - \frac{p_B \rho_0}{p_0} A_B \dot{x} \tag{7}$$

where ρ_0 and p_0 are the air density and pressure in reference conditions.

The air flow through the valves is given by

$$\dot{m} = \rho_0 C k_T \frac{\Delta p}{(1 - b)} \tag{8}$$

where $k_T = \sqrt{T/T_0}$ is the temperature ratio, b the critical ratio and C the valve conductance, Δp is the pressure difference between chambers. The pressure difference on the supply valve is $\Delta p = p_s - p$ and $\Delta p = p - p_a$ on the discharge valve, where p_s is the supply pressure and p_a is the ambient pressure, while p is the pressure in chambers.

The proportional valves model is linearized around the operating point defined by $(p_s+p_a)/2$. Neglecting the opening time of the valve, this expression results to be proportional to the command signal u to the valve:

$$\dot{m} = Ku\Delta p \tag{9}$$

Input signal u can change in range $-1<u<1$; positive/negative values refer to outward/backward cylinder motion.

From relations (3) to (9) it is possible to obtain the transfer function $G_{\theta/u} = \frac{\theta(s)}{u(s)}$ between input signal u and angle θ.

$$G_{\theta/u} = \frac{\theta(s)}{u(s)} = \frac{(K_A A_A + K_B A_B)s}{(M_p+m_c)ls^4+(b_c+b_p)ls^3+(C_A A_A+C_B A_B)ls^2-(M_p+m_c+m_p)gs^2-(b_c+b_p)gs-(C_A A_A+C_B A_B)g} \tag{10}$$

Moreover, the relationship between the force F available in output from actuator and variables u and x is made explicit, where the cart position is assimilated to a disturbance variable and u is the input variable:

$$F(s) = \frac{K_A A_A + K_B A_B}{s} u(s) - (M_p s^2 + b_p s + C_A A_A + C_B A_B)x(s) \tag{11}$$

where

$$K_A = p_0 \frac{K\frac{p_s}{2}}{\rho_0 V_{A0}}$$

$$K_B = p_0 \frac{K\frac{p_s}{2}}{\rho_0 V_{B0}}$$

$$K = \rho_0 C k_T$$

$$C_A = \frac{\frac{p_s}{2}}{V_{A0}} A_A$$

$$C_B = \frac{\frac{p_s}{2}}{V_{B0}} A_B$$

3 Control architecture

The control is aimed at controlling the pendulum angle and the cart position in the set point reducing to zero the error between set and feedback. The control on x is necessary as the cylinder stroke is limited to ±250 mm. Figure 1 outlines the block diagram of the control

architecture, which consists of a cascade of two loops to control angle θ (inner loop) and position x (outer loop).

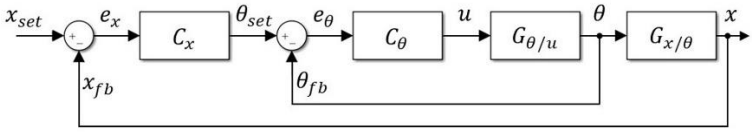

Fig. 1. Control system architecture only with θ and x controlled.

As an alternative to this scheme, a further loop is introduced to control the force F exerted by the cylinder on the cart. The new architecture is depicted in Figure 2. In this case, a load cell is inserted between cylinder and cart. The eventual advantages of introducing this loop are discussed here below.

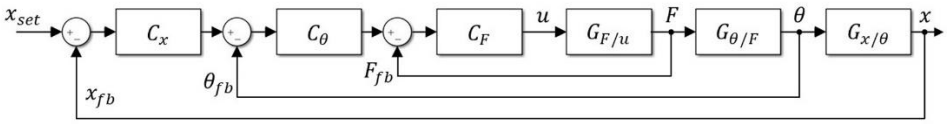

Fig. 2. Control system architecture with F, θ and x controlled.

4 The regulators

Referring to Figures 1 and 2, transfer functions C_x, C_θ, C_F are the regulators of displacement, angle and force loops respectively. The regulators designed are the filtered PID (with first order filter on the derivative part) and the filtered PD. The first one assumes the following form:

$$C_{PID_f}(s) = K_p + \frac{K_i}{s} + \frac{K_d s}{\tau_d s + 1}$$

where K_p, K_i, K_d are the proportional, integral and derivative gains, while τ_d is the filter time constant. The second one lacks of the integral part and is equivalent to a phase lead compensator.

For the angle loop, compensator C_θ was found to be of PIDf type. For the position loop, two alternatives compensators C_x were designed: a PIDf and a PDf.

5 Results and discussion

A stability analysis of the linearized system is performed around the operating point, characterized by x =0, θ =0.

The compensators of the control architecture of Figure 1 were designed with Matlab pid Tuner toolbox considering the following constraints: a) the crossover frequency of the inner angle loop was fixed to 10 rad/s; b) the crossover frequency of the displacement outer loop

was fixed to 1 rad/s; c) the minimum phase margin of both loops was set to 50°. Stability was verified both using the Nyquist criterion and analysing the sign of the closed loop transfer function roots.

5.1 Control architecture 1: angle θ and displacement x

Table 1. Compensators of x and θ loops

Compensator	type	K_p	K_i	K_d	τ_d	Gain Margin	Phase Margin
C_θ	PIDf	2.08	9.87	0.109	0.000875	5.33 dB @17.6rad/s	50° @10rad/s
C_x	PDf	-0.00702	-	-0.0467	0.285	10.9 dB @3.59rad/s	55.8° @1rad/s
C_x	PIDf	-0.00868	-0.000401	-0.0461	0.183	11.1 dB @4.31rad/s	59.1° @1rad/s

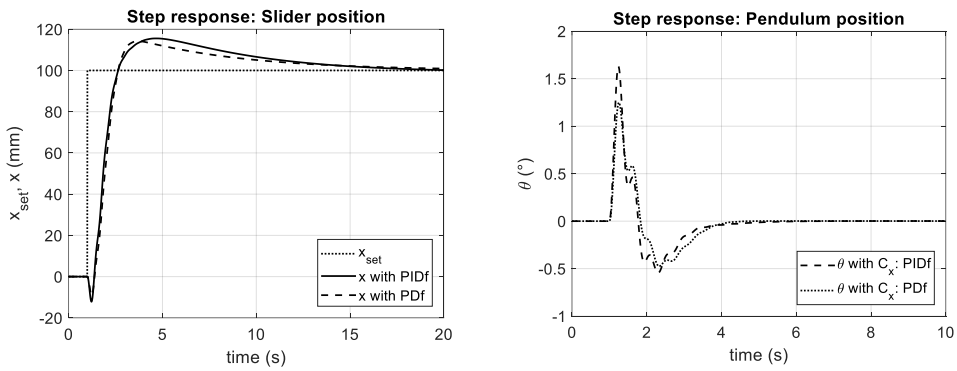

(a) (b)

Fig. 3. Response to a step displacement with two different compensators C_x, (a) cart position and (b) pendulum angle.

The performance of the controlled system is evaluated with the response to a displacement step. Figures 3a-3b show the cart displacement and the pendulum angle after a 100 mm step, considering the designed compensators C_x.

The settling time, evaluated to reach 2% of the static value, is 13.9 s and 13.6 s for the PDf and the PIDf respectively, while the overshoot is 14.2% and 15.5% respectively. In both cases the angular oscillations is limited in range ±2°, see Figure 3b.

5.2 Control architecture 2: force F, angle θ and displacement x

The force control is based on eq. (11), which describes the dependency on x, assimilated to a disturbance, and input signal u. The block diagram of Figure 4 depicts the force loop which have been considered to design compensator C_F.

Eq. (13) defines the disturbance transfer function between x and F, while eq. (14) expresses it in the normalized form.

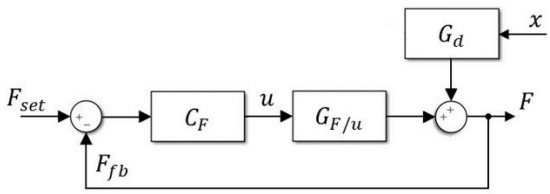

Fig 4. Control loop of the controlled variable F.

$$G_{F/u}(s) = \frac{K_A A_A + K_B A_B}{s} = \frac{G_1}{s} \tag{12}$$

$$G_d(s) = -(M_P s^2 + b_P s + C_A A_A + C_B A_B) \tag{13}$$

$$\begin{aligned} G_d(s) &= -(C_A A_A + C_B A_B)\left(\frac{M_P s^2}{C_A A_A + C_B A_B} + \frac{b_P s}{C_A A_A + C_B A_B} + 1\right) = \\ &= G_{2c}\left(\frac{s^2}{\sigma_d^2} + 2\zeta_d \frac{s}{\sigma_d} + 1\right) = G_{2c} G_2(s) \end{aligned} \tag{14}$$

where $\sigma_d \cong 33{,}5\, rad/s$ $\zeta_d \cong 0{,}63$. These parameters are only function of physical parameters of the system.

The closed loop transfer function is

$$F(s) = \frac{1}{\frac{1}{C_F G_1} s + 1} F_{set} + \frac{\frac{G_d}{C_F G_1} s}{\frac{1}{C_F G_1} s + 1} x \tag{15}$$

while the open loop transfer function (see Figure 4) is

$$C_F G_{F/u} = \frac{C_F G_1}{s} \tag{16}$$

The system stability is assured as the phase is always beyond -90°. Considering constant Fset, the variation of F due to a variation of disturbance x is expressed by

$$F(s) = \frac{\frac{G_d}{C_F G_1} s}{\frac{1}{C_F G_1} s + 1} x \tag{17}$$

while the disturbance stiffness is defined as the inverse function:

$$\frac{x}{F}(s) = \frac{1 + C_F G_{F/u}}{G_d} = \frac{C_F G_1 / G_{2c}}{s} \frac{\left(\frac{1}{C_F G_1} s + 1\right)}{G_2(s)} \tag{18}$$

It is important to have a high disturbance stiffness in order to have a negligible influence of the disturbance on the controlled variable. Figure 5 shows the Bode diagram of the disturbance stiffness: introducing the controller, it is clear that it remains high in a wide frequency range, sufficient to cover the frequency of variation of displacement x.

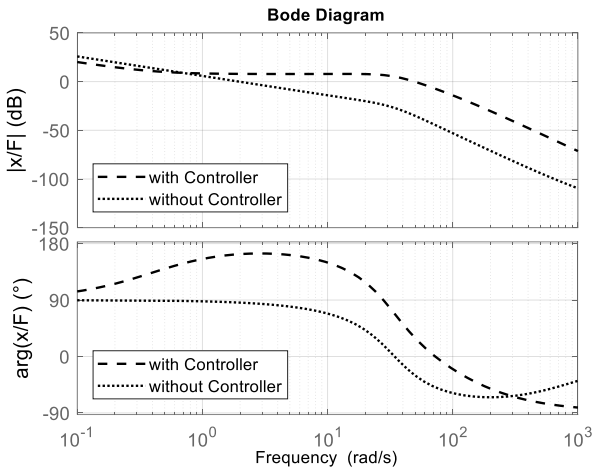

Fig. 5. Bode diagram of disturbance stiffness, with and without compensator C_F.

The adopted compensator is expressed by

$$C_F(s) = K_p + \frac{K_d s}{\tau_d s + 1} = 0.5 + \frac{1.24s}{0.01s + 1}$$

It gives wide stability margins and a crossover frequency higher than 100 rad/s. Compensators C_θ e C_x are also reported in Table 2.

Table 2. Compensators of x and θ loops in case of force control

Compensator		type	K_p	K_i	K_d	τ_d	Gain Margin	Phase Margin
C_θ	PIDf	88.8	218	8.99	0.000875		-11.9 dB @1.76rad/s	50° @10rad/s
C_x	PDf	-0.0149	-	-0.074	0.267		9.35 dB @5.77rad/s	64.9° @1rad/s
C_x	PIDf	-0.0159	-0.000805	-0.0751	0.369		10.7 dB @5.25rad/s	59° @1rad/s

Figure 6 shows the response to a 100 mm displacement step in terms of cart position and pendulum angle obtained with two different compensators C_x.

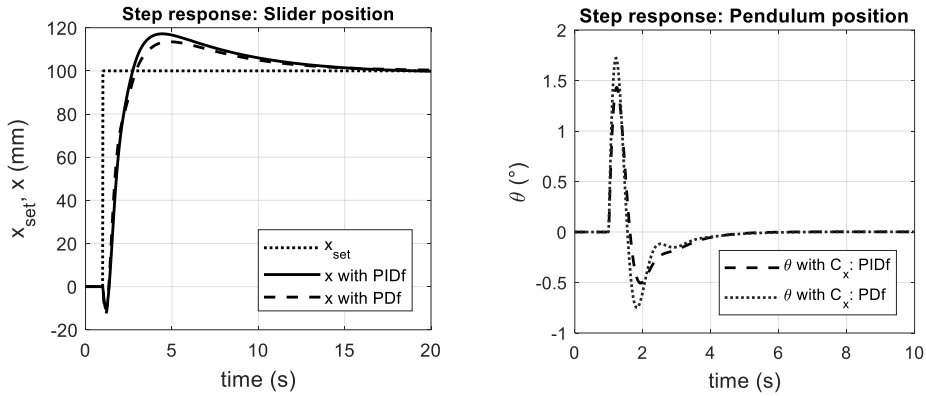

(a) (b)

Fig. 6. Step response with two different compensators C_x, (a) slider position and (b) pendulum position.

The settling time, evaluated to reach 2% of the static value, is 12.1 s and 12.7 s for the PDf and the PIDf compensators respectively, while the overshoot is 13.5% and 17.2% respectively. In both cases the angular oscillations is limited in range ±2°, see Figure 6b.

Comparison

In both control architectures the two proposed sets of compensators don't really differ. In architecture 2 (with the force loop) the settling time is a little smaller (-6,6%) considering the same type of compensator C_x.
Nevertheless, to have a more complete analysis of the comparison between the two architectures, a non-linear control system should be considered and experimental tests should be carried out.

6 Conclusions

Control architectures to stabilize a pneumatically actuated inverted pendulum were described in this paper and proper PD and PID compensators are designed. Cascade controls with two or three loops were considered to control the actuator force, the pendulum angle and the displacement. Both architectures allow the pendulum to be stable. In particular, the use of an additional internal force loop seems to be not so favorable in terms of transient response (settling time) compared to the cost needed for the force transducer. In order to further investigate and compare these solutions, a non-linear analysis will be carried out together with experimental tests.

Nomenclature

x: cart position (m)
θ: pendulum angle (rad)
A_A, A_B: cylinder sections (m^2)
C: valve conductance $\left(\frac{m^3}{sPa}\right)_{ANR}$
K: valve linearization coefficient (kg/sPa)

M_p: cylinder rod mass (kg)
T_0: temperature in reference conditions (K)
V_{A0}, V_{B0}: dead volumes of cylinder (m^3)
b_c: friction coefficient between cart and basement (Ns/m)
b_p: friction coefficient in cylinder (Ns/m)
l: pendulum length (m)
m_c: cart mass (kg)
m_p: pendulum mass (kg)
p_0: reference pressure (Pa)
p: absolute pressure (Pa)
p_a: ambient pressure (Pa)
ρ_0: air density in reference conditions (kg/m^3)
u: valve command signal
σ_d: damped natural frequency
ζ_d: damping ratio

References

1. https://it.wikipedia.org/wiki/Segway
2. https://en.wikipedia.org/wiki/Self-balancing unicycle
3. http://litmotors.com/
4. F. Grasser, A. D'Arrigo, S. Colombi, A. C. Rufer, *IEEE Transactions on Industrial Electronics*, **49** (1), pp.107-114 (2002).
5. N.M. Abdul Ghani, D. Ju, H.Z. Othman, M.A. Ahmad, Proceedings on *10th International Conference on Intelligent Systems Design and Applications*, pp. 1066-1070, IEEE, Cairo, Egypt, (2010).
6. H.W. Kim, S. Jung, *Robotica* (2016); **34** (5): pp. 1186–1208.
7. J.J. Wang, *Simulation Modelling Practice and Theory* (**19**), pp. 440–449 (2011).
8. L., Wende, D. Hui, C. Kai, Proceedings of *International Conference on Control 2012*, pp. 190-196. IEEE, Cardiff, UK (2012).
9. S. Kajita, M. Morisawa, K. Miura, S. Nakaoka, *IEEE Int. Conf. on Intelligent Robots and Systems*, pp. 4489-4496, Taipei, Taiwan, (2010).
10. B. Ugurlu, C. Doppmann, M. Hamaya, P. Forni, T. Teramae, T. Noda, J. Morimoto. *IEEEASME Transactions on Mechatronics*, **21** (1), pp. 79-87 (2016).
11. T. Žilić, D. Pavković, D. Zorc. *ISA Transactions* **48** (3), pp. 327-335 (2009).
12. C. Krupke, J. Wang. International Proceedings of the *Conference on Advanced Intelligent Mechatronics*, pp. 812-817. IEEE, Busan, Korea (2015).
13. F. Colombo, L. Mazza, G. Pepe, T. Raparelli, A. Trivella, *RAAD 2018*, Mechanisms and Machine Science, **67** (2018).
14. M. Pontin, F. Colombo, L. Mazza, T. Raparelli, *Proc IMechE* Part I: J. Systems and Control Engineering, pp. 1-12 (2019).
15. L. Mazza, G. Belforte, *ASME. J. Tribol.*, **139**(2) 022202 (2017).